Applied Energy 161 (2016) 92–100

Contents lists available at ScienceDirect

Applied Energy

journal homepage: www.elsevier.com/locate/apenergy

Kinetics of oxygen uncoupling of a copper based oxygen carrier

Wenting Hu [a,*], Felix Donat [a], S.A. Scott [b], J.S. Dennis [a]

[a] Department of Chemical Engineering and Biotechnology, University of Cambridge, Pembroke Street, Cambridge CB2 3RA, United Kingdom
[b] Department of Engineering, University of Cambridge, Trumpington Street, Cambridge CB2 1PZ, United Kingdom

HIGHLIGHTS

- The kinetics of a Cu-based oxygen carrier was determined using a TGA.
- A diffusion model was applied to remove mass transfer effects from rate parameters.
- Thermodynamics are separated from kinetics, usually difficult for the CLOU reaction.
- The rate parameters correctly described the behaviour in a fluidised bed.
- The rate parameters can be used to predict performance of large CLOU systems.

ARTICLE INFO

Article history:
Received 19 April 2015
Received in revised form 30 September 2015
Accepted 1 October 2015
Available online 22 October 2015

Keywords:
Chemical-looping
CLOU
Oxygen carrier
Mass transfer
Kinetics

ABSTRACT

Here, an oxygen carrier consisting of 60 wt% CuO supported on a mixture of Al_2O_3 and CaO (23 wt% and 17 wt% respectively) was synthesised by wet-mixing powdered CuO, $Al(OH)_3$ and $Ca(OH)_2$, followed by calcination at 1000 °C. Its suitability for chemical looping with oxygen uncoupling (CLOU) was investigated. After 25 repeated redox cycles in either a thermogravimetric analyser (TGA) or a laboratory-scale fluidised bed, (with 5 vol% H_2 in N_2 as the fuel, and air as the oxidant) no significant change in either the oxygen uncoupling capacity or the overall oxygen availability of the carrier was found. In the TGA, it was found that the rate of oxygen release from the material was controlled by intrinsic chemical kinetics and external transfer of mass from the surface of the particles to the bulk gas. By modelling the various resistances, values of the rate constant for the decomposition were obtained. The activation energy of the reaction was found to be 59.7 kJ/mol (with a standard error of 5.6 kJ/mol) and the corresponding pre-exponential factor was 632 m^3/mol/s. The local rate of conversion within a particle was assumed to occur either (i) by homogeneous chemical reaction, or (ii) in uniform, non-porous grains, each reacting as a kinetically-controlled shrinking core. Upon cross validation against a batch fluidised bed experiment, the homogeneous reaction model was found to be more plausible. By accurately accounting for the various artefacts (*e.g.* mass transfer resistances) present in both TGA and fluidised bed experiments, it was possible to extract a consistent set of kinetic parameters which reproduced the rates of oxygen release in both experiments.
© 2015 The Authors. Published by Elsevier Ltd. This is an open access article under the CC BY license (http://creativecommons.org/licenses/by/4.0/).

1. Introduction

Chemical-looping combustion is a promising alternative to conventional combustion with the inherent ability to produce a flue gas composed of almost pure CO_2, thereby reducing the cost for carbon capture and minimising the loss in plant efficiency [1,2]. The technology typically utilises suitable solid materials as oxygen carriers to transport oxygen for combustion between two interconnected fluidised bed reactors (the fuel reactor, where combustion takes place, and the air reactor where the oxygen carriers are regenerated) and avoids the direct contact between fuel and air [3–10]. Chemical-looping with oxygen uncoupling (CLOU), as a special case of chemical-looping combustion, involves the use of oxygen carriers capable of releasing gas-phase oxygen at high temperatures [11–15]. This is advantageous for applications involving solid fuels since the gaseous oxygen is able to react with both the volatile and involatile components of the fuel directly. This contrasts with conventional chemical looping where it is necessary to first gasify the char to synthesis gas which is generally rate-limiting. Therefore, in the CLOU processes, char conversion is fast and the fuel reactor can be made smaller for a given heat duty [14]; and the carry-over of char into the air reactor is minimised. The fate of the char and avoiding carry-over into the air reactor

* Corresponding author.
E-mail address: wh254@cam.ac.uk (W. Hu).

http://dx.doi.org/10.1016/j.apenergy.2015.10.006
0306-2619/© 2015 The Authors. Published by Elsevier Ltd.
This is an open access article under the CC BY license (http://creativecommons.org/licenses/by/4.0/).

is critical for the future development of chemical looping combustion, since carbon combusted the air reactor is released into the environment, decreasing the capture efficiency [16,17].

Oxygen carriers which can release gas phase oxygen include oxides of copper, cobalt, manganese [11,18–20] and more complex mixed oxides such as spinels [10,21–23] or perovskites [24–26]. Oxygen carriers based on copper oxide have a very high oxygen carrying capacity, up to 10 wt%. Furthermore, the oxygen release from CuO is only moderately endothermic and when combined with the combustion of the fuel, results in an overall exothermic reaction in the fuel reactor. The equilibrium partial pressure of oxygen for reaction (1), P_{eq}, increases from 0.0048 to 0.047 bar at typical operating temperatures between 850 °C and 950 °C, respectively [27].

$$4CuO \leftrightarrow 2Cu_2O + O_2 \quad (1)$$

From an operational point of view, this moderate equilibrium partial pressure of oxygen is important: too low a P_{eq} means the CLOU effect is lost and with much higher P_{eq}, the loss of oxygen in the during the conveying of the freshly-oxidised carrier from the air reactor to the fuel reactor would be significant, thereby diminishing the effective oxygen carrying capacity of the carrier. Furthermore, if P_{eq} exceeded 0.21 bar, it would not be possible to re-oxidise the carrier with air at atmospheric pressure at all, a significant drawback.

Considering potential scale up, copper based materials, like those considered here, have found favour owing not only to the favourable properties of the copper oxides, but also because of cost, and the relatively low toxicity of copper compounds compared to, say, cobalt oxides. Many studies [3,28–31] have shown that copper-based oxygen carriers can retain full oxygen carrying capacity over many redox cycles as well as offer reasonable resistance towards attrition and agglomeration for operation in fluidised beds [23,32] and continuous operation with such carriers has been demonstrated in small-scale fluidised bed systems [33]. The resistance to agglomeration and long term stability in the oxygen carrying capacity, both essential for scale up, requires the copper to be supported/mixed with other oxide materials [31,34,35]. In this work, copper oxides supported with alumina are considers, since previous studies have shown that stable oxygen carrying capacity can be achieved with similar materials [36].

The low oxygen partial pressures achievable using reaction (1) do not pose a problem, since in CLOU combustion in a fluidised bed the oxide is in intimate contact with the fuel and can be consumed locally as it is produced [31]. The kinetics of reaction (1) are of crucial importance since as the fuel burns, the oxygen is removed from the vicinity of the oxygen carrier causing release of further oxygen, *i.e.* the rate of combustion of the fuel can be limited by the rate at which oxygen can be released from the oxygen carrier, not the overall oxygen partial pressure it could produce. Therefore, accurate knowledge of the kinetics of the oxygen carrier used is a prerequisite for the proper design of CLOU reactors. Despite the importance of understanding the kinetics of reaction (1), investigations of the kinetics of the oxygen uncoupling have been inconclusive so far, largely owing to the difficulties in making measurements of what is essentially a very fast reaction, which is often limited by chemical equilibrium and/or mass transfer. Arjmand et al. [31] used a bed of wood char to remove the gaseous oxygen released by the carrier to keep the ambient partial pressure of oxygen low and measured an apparent activation energy of 139.3 kJ/mol for the decomposition of CuO supported on $MgAl_2O_4$. Sahir et al. [37] proposed that the apparent activation energy should be separated into a thermodynamic driving force of approximately 260 kJ/mol, corresponding to the enthalpy of reaction, and the true activation energy from the intrinsic kinetics. They analysed the kinetic data obtained from combustion of Mexican petcoke with CuO supported on ZrO_2 [11,12] and found the true activation energy to be about 20 kJ/mol. Following a similar argument, Clayton and Whitty [29] concluded that the true activation energy of the reduction of two different supported CuO particles were significantly higher, at 58 kJ/mol and 67 kJ/mol respectively and the activation energy of the oxidation of the same carriers in reduced form were found to be 43 kJ/mol and 69 kJ/mol [38].

In this work, the oxygen carrier was prepared by simple mixing and sintering of the component hydroxides to make the oxygen carrier production method easier to scale than, *e.g.* co-precipitation from soluble nitrate salts or sol–gel techniques [30,39]. The chosen method also minimises the interaction between the support and the copper oxide, and minimises the introduction of contaminants such as sodium which could affect the behaviour of the resulting particles [40,41]. Since the kinetic information for reaction (1) is critical for the design and effective operation of CLOU processes, the current work aims to determine the kinetics of the oxygen uncoupling via experiments and modelling. More generally, the difficulties in obtaining reliable kinetic information and some of the subtleties in determining the kinetics for reaction (1) are discussed.

2. Experimental

2.1. Materials

2.1.1. Preparation of the oxygen carrier

The oxygen carrier investigated in this work was produced by mixing 17.60 g $Al(OH)_3$ (Sigma–Aldrich, reagent grade) and 11.23 g $Ca(OH)_2$ (Fisher Scientific, >98%) powders with 400 ml of de-ionised water on a hot plate for 2 h, followed by the addition of 30.00 g of CuO (Sigma–Aldrich, <10 μm, 98%) and stirring for a further 20 h. The resulting mixture was dried at 80 °C for 48 h, crushed and the resulting granular material calcined at 1000 °C for 6 h. The cooled, calcined particles were sieved to 300–425 μm for subsequent use.

2.1.2. Characterisation of the oxygen carrier

XRD analysis of the oxygen carriers was performed using an Empyrean PANalytical diffractometer (Cu Kα, 40 kV, 40 mA) with a scan range of 5–80° and a step size of 0.0167°. The BET surface area, and BJH pore size distribution for pores <200 nm diameter, were determined from nitrogen adsorption experiments at 77 K using a TriStar 3000 (Micrometrics, Serial No. 1001) gas adsorption analyser.

2.2. Stability of the oxygen carrier

The chemical stability of the oxygen carrier was investigated using a thermogravimetric analyser (TGA) (Mettler-Toledo TGA/DSC1). In a typical experiment to investigate oxygen uncoupling and coupling (*viz.* the forward and reverse of reaction (1)), ~30 mg of the oxygen carrier was placed in an alumina crucible (70 μl capacity) across which was passed 55 ml/min of compressed air from a gas cylinder (BOC), introduced 2 mm above the top of the crucible and 9 mm away from its centre, in a background of 245 ml/min purge gas of compressed N_2 (both measured at 293 K and 1 atm total pressure). The temperature of the furnace of the TGA was changed from 900 °C to 1050 °C and then back to 900 °C at a rate of 2 °C/min five times to examine the consistency of oxygen uncoupling. In a typical experiment to examine both uncoupling and reduction of the product Cu_2O, ~20 mg of the sample was examined at 900 °C. The reactive gas (55 ml/min each at 293 K, 1 atm) was changed successively from nitrogen (for oxygen uncoupling) to 5 vol% hydrogen in nitrogen (for reduction of Cu_2O

to metallic copper) and finally to compressed air (for complete re-oxidation to CuO) for 10 min each, by means of a solenoid valve manifold (Burkert Type 6011) controlled by a separate programme synchronised with the TGA. This cycle of gases was repeated 25 times. A background flow of nitrogen (130 ml/min at 293 K, 1 atm) was always present to purge the furnace.

2.3. The kinetics of the decomposition of CuO to Cu_2O

To understand the kinetics of the oxygen carriers better, CLOU experiments were conducted between 850 °C and 950 °C at isothermal conditions in a TGA. In a typical experiment, between 6 and 10 mg of fully-oxidised sample was placed in a crucible. The sample was first heated in air (with argon as the background, at 140 ml/min, 293 K and 1 atm) to 900 °C. When the temperature had stabilised, the air was switched off and the decomposition reaction was allowed to proceed to completion with the TGA purged with Ar. The sample was then re-oxidised in air and the process was repeated five times to confirm that the behaviour of the particles was similar over cycles. Subsequently the particles were brought to 875 °C, 925 °C, 950 °C and 850 °C for a further redox cycle at each temperature.

A model was constructed, as described in Section 3.3.1, to extract the apparent activation energy of the reaction.

To confirm the validity of the kinetic parameters extracted in Section 3.3, an electrically-heated batch fluidised bed with an internal diameter of 17 mm, containing 8.0 g of silica sand (300–355 μm) was used. In a typical experiment, the bed was fluidised by a constant stream of nitrogen between 0.6 and 2.2 l/min, measured at 293 K and 1 atm. The temperature of the bed, measured by a type-K thermocouple immersed in the sand, was set between 850 °C and 950 °C. The experiment involved dropping approximately 10 mg of pre-cycled, fully oxidised oxygen carrier into the fluidised bed from above. A universal exhaust gas oxygen sensor (UEGO) with a response time of ~20 ms was used to sample the gas from the freeboard and measure its oxygen content. The details regarding the UEGO sensor are described elsewhere [42,43].

3. Results

3.1. Characterisation of the oxygen carrier

The oxygen carrier had a nominal composition of 60 wt% CuO, 23 wt% Al_2O_3 and 17 wt% CaO. XRD analysis of carriers both virgin and particles cycled isothermally at 900 °C for 5 times (hereafter as used particles) confirmed that the dominant phases present are CuO and $Ca_{12}Al_{14}O_{33}$, with only a trace amount of $CaAl_2O_4$. The virgin sample had a BET surface area of 0.949 m^2/g and a BJH pore volume of 2.34 mm^3/g for pore diameters ⩽200 nm, whereas the corresponding values for the sample after isothermal cycling were 0.810 m^2/g and 2.11 mm^3/g. The bulk density of the virgin sample was found to be 980 kg/m^3 and that of the cycled sample 1100 kg/m^3. The estimated particle densities, assuming the particles formed a close-packed bed with voidage of ~0.36, were 1500 kg/m^3 and 1700 kg/m^3 respectively. Taking the density [44] of $Ca_{12}Al_{14}O_{33}$ as 2680 kg/m^3 and that of CuO [45] as 6480 kg/m^3, the particle voidage ε_p was calculated to be ~0.70 for the virgin particles and ~0.66 for the cycled particles.

3.2. Chemical stability of the oxygen carrier

3.2.1. Temperature programmed reaction in an atmosphere of constant composition

A mass of 29.5 mg of oxygen carrier was investigated in the TGA using the protocol in Section 2.2 for oxygen uncoupling and coupling by changing the temperature of the furnace from 900 °C to 1050 °C and back at 2 °C/min for five repeated cycles.

Results are shown in Fig. 1. The decomposition of the oxygen carrier began at ~986 °C and the re-oxidation commenced at ~970 °C, as noted by the first detectable rate of change in mass of the sample, ~0.2 μg/s. The observed profiles of rate of change of mass *vs.* time during both release and uptake of oxygen were identical for cycles 2–5. The virgin material on cycle 1 showed some anomalous behaviour, not seen in subsequent cycles.

For cycles 2–5, the overall change in mass was found to be 1.864 mg, 1.862 mg, 1.861 mg and 1.862 mg, respectively, corresponding to a change of 6.3% of the total mass of the carrier, slightly higher than the expected value of 6.0%, based on the stoichiometry of the starting material.

To gauge whether or not the rates shown in Fig. 1 are dominated by mass transfer effects in the TGA external to the heap of particles, an estimate of the rate of external mass transfer was made, as follows. The arrangement of the reacting particles in the crucible of the TGA resembles that of a Stefan tube as illustrated in Fig. 2. Considering the case when the carrier is decomposing, the Stefan-Maxwell equation can be applied to the flux of the binary mixture of nitrogen and oxygen in the crucible between the external surface of the particles and the upper lip of the crucible, at an average height L above the bed of particles. In this initial analysis, the mole fraction at the external surface of the particles, $y_{r,s}$ was taken to be that at thermodynamic equilibrium and the mole fraction at the lip constant and equal to that of the bulk gas mixture, $y_{r,b}$, passing through the TGA. Transfer within the crucible is taken to be purely by diffusion and advection, without any fluid dynamic effects. Noting that the flux of nitrogen must be zero in the crucible, it is readily shown that at steady state, the molar flux of oxygen from the surface of the oxygen carrier to the top of the crucible is

$$N_r = \frac{cD}{L}\ln\left(\frac{1-y_{r,b}}{1-y_{r,s}}\right) \tag{2}$$

where the total molar concentration of gas, assumed constant, is c and the binary molecular diffusivity for oxygen and nitrogen is D. In Eq. (2), the bulk concentration of oxygen flowing across the top of the crucible was estimated using

$$y_{r,b} = \frac{0.209F_r}{F_r + 0.5F_p} \tag{3}$$

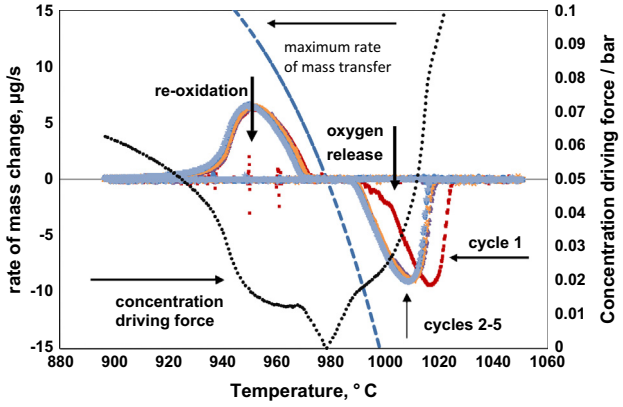

Fig. 1. Rate of mass change of 5 cycles of temperature programmed reaction (left axis). The calculated maximum rate of external mass transfer (dashed line, left axis) and the concentration driving force for cycle 5 (dotted line, right axis) are also included for comparison.

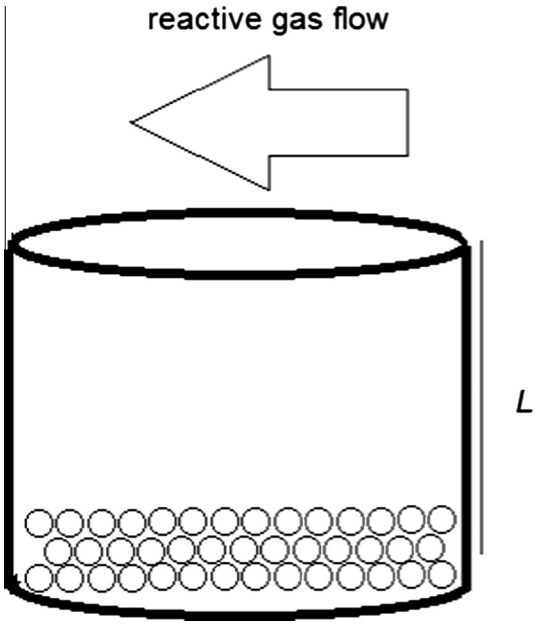

Fig. 2. Illustration of a TGA crucible containing oxygen carrier particles.

where F_r and F_p were the molar flowrates of the reactive and purge gases, respectively. The factor of 0.5 was introduced to correct for the fact that only about half the purge gas was mixed with the reactive gas as it blew across the crucible. This value was estimated by assuming that the partial pressure of oxygen in the bulk gas was equal to P_{eq} at 978 °C, midway between the onset of decomposition and re-oxidation. Given that the heating rate of the TGA was very low, at 2 °C/min, it was reasonable to assume that the temperature gradient between the sample particles and the furnace was negligible and did not affect the derivation of Eq. (2). The crucible used was a cylinder with a depth of 4 mm and internal diameter 4.9 mm. The value of L was taken as the average distance from the surface of individual particles to the lip of the crucible, ~3.5 mm. Binary diffusion coefficients were obtained using the Fuller-Schettler-Giddings equation [46].

The maximum rate of mass transfer was calculated using Eq. (2), taking the concentration of oxygen at the surface of the particles to be P_{eq}. The resulting flux was multiplied by the area of the crucible and the molar mass of oxygen to yield the theoretical maximum rate of mass change, as shown in Fig. 1. It can be seen that the maximum rate of external mass transfer was of the same order of magnitude as the rate of reaction, suggesting that it has a significant, but not overwhelming, influence on the rates of decomposition and oxidation observed experimentally.

Furthermore, assuming quasi-steady-state conditions, the diffusive flux should be equal to the rate of reaction divided by the cross sectional area of the crucible. Values of $y_{r,s}$ and hence the corresponding partial pressure of oxygen at the surface of the particles, were calculated using Eq. (2), with the measured molar flux as input. The concentration driving force shown in Fig. 1 was then derived as the difference between the partial pressure of oxygen at the surface of the particles and the equilibrium partial pressure of oxygen at given temperatures. During the reactions, the minimum driving force at the surface was about 0.012 bar.

3.2.2. Isothermal cycling experiment

To confirm that the oxygen carrier could retain activity over repeated use, including reduction of the Cu_2O at the end of the thermal decomposition of CuO, 21.05 mg of the particles were investigated at 900 °C in the TGA for 25 cycles using the protocol described in Section 2.2. The results are shown in Fig. 3 as observed rate of change of mass during (a) decomposition in nitrogen, (b) reduction with hydrogen and (c) re-oxidation in air.

From the curves in Fig. 3, it was found that the total amount of oxygen available from the carrier, measured by the mass change in the re-oxidation stage, remained consistently at 2.596 ± 0.002 mg, corresponding to 12.4% of the total mass of the carrier. Furthermore, the profiles of rate of mass change in each stage were identical across cycles with the exception of the first cycle, which showed a slower rate in the oxygen release stage. Using Eqs. (2) and (3), the maximum rate of mass transfer was calculated for each stage in the cycle and was found to be of the same order of magnitude as the maximum observed rate of reaction. Of course, the fact that the rate of reaction in each case varied with conversion at isothermal conditions suggests that the reactions were not entirely controlled by external mass transfer. Thus, the reproducibility of the reaction rate profile over cycles can be attributed to the structural stability of the particles.

From Fig. 3, it is also worth noting that the re-oxidation appears to occur via a two-step process, evident from the plateau-like feature of the apparent rate at $t \sim 1255$ s. This feature coincides with the point of 50% conversion for the 5th and 25th cycles, shown in Fig. 3(c) by the dotted vertical line. When the experiment was repeated with a lower bulk oxygen concentration, the feature became more pronounced, due to a smaller concentration driving force for the oxidation of Cu_2O.

3.3. The kinetics of the decomposition of CuO to Cu_2O

To characterise the oxygen carrier particles further, isothermal experiments were conducted in the TGA between 850 °C and 950 °C following the protocol outlined in Section 2.3. The particles were cycled isothermally at 900 °C five times in order to eliminate the abnormal behaviour on the first cycle, observed in Section 3.2.

3.3.1. Coupling particle kinetics with external mass transfer

It was established in Section 3.2 that external mass transfer was significant in the TGA. Therefore, when extracting kinetic parameters, the effect of mass transfer has to be taken into account. In the following, the decomposition of CuO in Reaction (1) is considered.

To start with, consider the case where the diameter of the particles is sufficiently small that there is no intraparticle resistance to mass transfer and so, within the particle, the reaction is controlled by intrinsic chemical kinetics. For a monodispersed batch of particles in a single layer at the base of the crucible, the molar flux of oxygen, N_r, at some height in the crucible is equal to the rate of reaction of the particles per unit cross-sectional area of crucible, A:

$$N_r = \frac{n}{A}\frac{\rho_m \pi r_0^3}{3} k_i (C_{eq} - C_s) f(X) \equiv k_i' (C_{eq} - C_s) f(X) \tag{4a}$$

where n is the number of particles in the crucible, ρ_m the molar density of CuO in the particle and r_0 the radius of a single oxygen carrier particle. This equation allows for the stoichiometry of Reaction (1). The rate of conversion of n particles in terms of oxygen released is $-\frac{1}{4}\frac{d}{dt}\left(\frac{n\rho_m 4\pi r_0^3}{3}(1-X)\right)$, and the rate of conversion per unit volume of the particles is given by

$$\frac{dX}{dt} = k_i (C_{eq} - C_s) f(X) \tag{4b}$$

where k_i is the intrinsic rate constant, C_{eq} the equilibrium concentration of oxygen at the reaction temperature, C_s the concentration of gas phase oxygen at the surface of the particles and $f(X)$ the functional form of the dependence of intrinsic reaction rate on conversion, X.

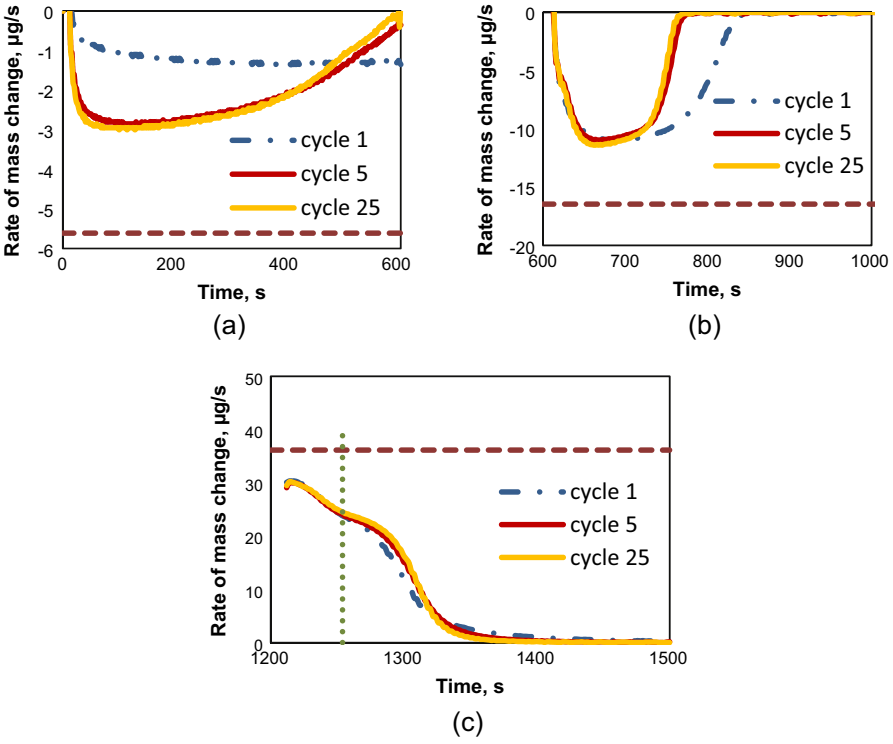

Fig. 3. Rate of change of mass of sample for selected cycles. (a) Oxygen release in N_2 (0–600 s); (b) reduction in 5% H_2 (600–1200 s); (c) re-oxidation in air (1200–1800 s). Dashed lines: maximum rate of external mass transfer, calculated as in Section 3.2.1. The dotted vertical line in graph (c) indicates the time when 50% conversion has been reached for the 5th and 25th cycles. The initial 12 s of data for each section (large mass fluctuations due to gas switching) have been omitted for clarity.

Referring back to the development of Eq. (2), the mass transfer coefficient can be approximated as $k_g \approx D/L$ when $y_{r,b}$ and $y_{r,s}$ are small. Since the equilibrium partial pressure of oxygen for the system at 950 °C is about 0.05 bar, the error associated with the approximation would be no more than 3%. Thus, at quasi-steady-state, Eq. (2) becomes:

$$N_r \approx k_g(C_s - C_b). \tag{5}$$

Here, C_b is the concentration of oxygen in the bulk gas, *i.e.* at the lip of the crucible.

It has been suggested that the oxidation of Cu_2O to CuO can be modelled with a homogeneous reaction model at temperatures above 800 °C [38], *i.e.* $f(X) = 1 - X$, assuming reduction follows the same model, Eq. (4a) becomes

$$N_r = \frac{n}{A}\frac{\rho_m \pi r_0^3}{3} k_i(C_{eq} - C_s)(1 - X) = k_i'(C_{eq} - C_s)(1 - X) \tag{6}$$

Assuming the process is at quasi-steady-state, C_s can be eliminated from Eqs. (5) and (6) to give

$$C_s = \frac{k_i'(1 - X)}{k_i'(1 - X) + k_g}(C_{eq} - C_b) + C_b \tag{7}$$

so that

$$N_r = \frac{k_i'(1 - X)k_g}{k_i'(1 - X) + k_g}(C_{eq} - C_b) \tag{8}$$

or

$$1/N_r = \frac{1}{k_i'(C_{eq} - C_b)(1 - X)} + \frac{1}{k_g(C_{eq} - C_b)}. \tag{9}$$

Thus a plot of $1/N_r$ against $1/(1 - X)$ should allow the extraction of $k_i'(C_{eq} - C_b)$ and $k_g(C_{eq} - C_b)$ independently, with the ratio of the intercept to the gradient of the plot yielding k_i'/k_g.

3.3.2. Effect of particle size on rate of reaction

Eq. (6) was postulated assuming that the reaction occurs uniformly throughout the particle. Whilst this is likely to be true for small particles, as the particle size increases, the effect of internal mass transfer will become important and a shrinking core, or diffuse reaction zone model would then be more appropriate. To investigate the effect of particle size on the rate of reaction, two samples of about 10 mg each were reduced at 900 °C under identical conditions in the TGA. The first sample contained particles with sizes between 300 and 425 μm, whereas the second sample contained particles with sizes between 100 and 160 μm. Results are shown in Fig. 4. It can be seen that the profile of rate against conversion was very similar for the two samples, and the time taken for complete conversion was comparable. The fact that the reaction

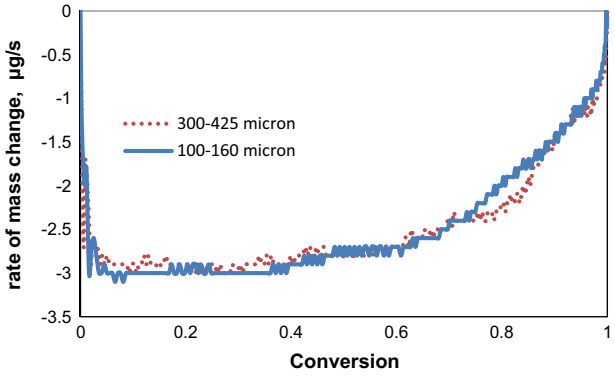

Fig. 4. Rate of oxygen release of two samples with comparable mass but different particle sizes in argon at 900 °C. An alumina crucible with depth 4 mm and diameter 4.9 mm was used. 300–425 μm sample: 10.4 mg, time for completion: 280 s; 100–160 μm sample: 9.8 mg, time for completion: 270 s.

is not influenced by particle size suggests that with a particle size up to 425 μm, the effect of internal mass transfer is not significant. Had both batches been in the regime of significant intraparticle mass transfer, there would have been a difference in rate, because the effectiveness factors would have been different for the two sizes. Finally, evidence from determining the activation energy, discussed in Section 3.3.4 below, is strongly in favour of the particles operating without substantial intraparticle mass transfer.

3.3.3. Effect of particle–particle interaction

To minimise the influence of neighbouring particles, care was taken to ensure that a monolayer of oxygen carrier particles was used for experiments. To confirm that the presence of other oxygen carrier particles did not influence the reaction of a single particle significantly, two samples (300–425 μm) of similar mass (6.5 mg *vs*. 6.3 mg) were decomposed in argon at 900 °C under identical conditions in the TGA except that the second sample was mixed with quartz sand particles of the same size fraction to increase the inter-particle spacing. The time for complete reaction and the rate profile were found to be identical allowing for experimental errors and it was concluded that neighbouring particles do not have a significant effect on the reaction of a single particle.

3.3.4. Determination of the apparent rate constants

From Eq. (9), it can be seen that although $k_i'(C_{eq} - C_b)$ and $k_g(C_{eq} - C_b)$ can be obtained from a plot of $1/N_r$ against $1/(1 - X)$ independently, a small value of k_g could still dominate the reaction and mask the kinetics of the particle until a very high conversion is reached. This would result in a decrease in the number of useful data points that could be obtained from a particular experiment and, in extreme cases, introduce large errors in the value of k_i'. Therefore, the shallowest crucible available, with a height of 2.1 mm and diameter 5.5 mm (the typical alumina crucible used had a depth of 4 mm and diameter 4.9 mm) was used to extract kinetic information, in order to minimise the effect of external mass transfer.

A modified Arrhenius plot of the results obtained from 850 °C to 950 °C, following the procedure outlined earlier, is presented in Fig. 5. In constructing Fig. 5, the dependence of k_g on temperature was accounted for by the inclusion of the correction factor $(T/1123)^{1.75}$. From Fig. 5, the apparent activation energy was found to be 59.7 kJ/mol with a standard error of 5.6 kJ/mol. The corresponding pre-exponential factor for k_i is 632 m^3/mol/s. The fact that the activation energy is in very good agreement with the results from Clayton et al. [29] further supports the assertion made in Section 3.3.2 that the particles did not have significant intra-particle transfer resistance. Had they possessed a substantial effectiveness factor, the derived value of 59.7 kJ/mol would have been one half the true value and substantially outside the range quoted by Clayton et al. [29].

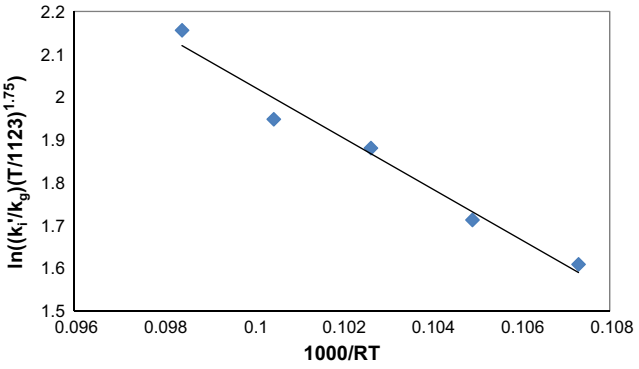

Fig. 5. Modified Arrhenius plot for data obtained at 850 °C, 875 °C, 900 °C, 925 °C and 950 °C, values of k_i' and k_g are extracted using data between 20% and 90% conversion at each temperature. Particle size 300–425 μm, sample mass 6.13 mg. The activation energy was found to be 59.7 ± 5.6 kJ/mol, with a coefficient of determination of 0.974.

The values of k_i'/k_g were found to range from 5.0 and 7.4, confirming that external mass transfer is important in the TGA, but not so large as to render it impossible to measure the intrinsic rate parameters.

3.3.5. Comparison between model and experimental results

3.3.5.1. Change in sample mass and external mass transfer. To investigate the validity of the model further, it was used to compare theory with experiment for two cases. In the first, a different crucible was used in the TGA (depth 4 mm and diameter 4.9 mm) so that the external mass transfer coefficient k_g was altered; in the second case, a larger mass of sample (9.84 mg) was used in addition to the change in crucible. Both experiments were carried out at 900 °C with pre-cycled materials, in the size range 300–425 μm and results are shown in Fig. 6. It can be seen that the model is able to predict both cases well. It is worth noting that the experiment with a larger mass showed a more severe external mass transfer limitation up to about 80% conversion and a sharper change in rate towards the end of reaction and this is captured by the model.

4. Discussion

Whilst the experimental results from Section 3.3 fitted well with a homogeneous reaction model, it should be noted that an equally good fit could be obtained with a shrinking grain model – that is, assuming the particles contained fine grains of CuO dispersed evenly throughout the particle with each grain following a shrinking-core reaction model. In this case, Eq. (4b) becomes

$$\frac{dX}{dt} = k_{i,s}(C_{eq} - C_s)(1 - X)^{2/3}. \tag{10}$$

where $k_{i,s}$ is a surface-based rate constant, proportional to k_i, with a corresponding activation energy of 79.2 ± 2.8 kJ/mol and a pre-exponential factor of 1350 m^3/mol/s. It is difficult to distinguish between the two models in the TGA because of the significant contribution from external mass transfer. To circumvent this, some batch experiments were carried out in a fluidised bed, where the rate of external mass transfer was faster. The experimental arrangement was described in Section 2.3 and Fig. 7 displays a typical batch experiment conducted at 904 °C.

In order to utilise and compare the kinetic parameters, a model of the fluidised bed was required. Here, the fluidised bed was modelled as having a bubble phase in plug flow with a well mixed particulate phase. The cross flow between the particulate phase and bubble phase was estimated using a correlation proposed by Sit and Grace [47],

$$k_{gt} = \frac{U_{mf}}{3} + \sqrt{\frac{4D\varepsilon_{mf}u_b}{\pi d_b}} \tag{11}$$

where k_{gt} is the interphase mass transfer coefficient, U_{mf} is the incipient fluidisation velocity estimated using the correlation by Wen and Yu [48], D is the diffusivity of gas, and ε_{mf} is the voidage in the particulate phase, measured as 0.42 at room temperature and assumed to be independent of temperature. The bubble velocity, u_b, is related to the bubble diameter d_b via [49]

$$u_b = 0.711\sqrt{gd_b} + U_0 - U_{mf} \tag{12}$$

where g is the gravitational acceleration and U_0 is the superficial gas velocity through the bed. The bubble diameter d_b can be found by using [50]

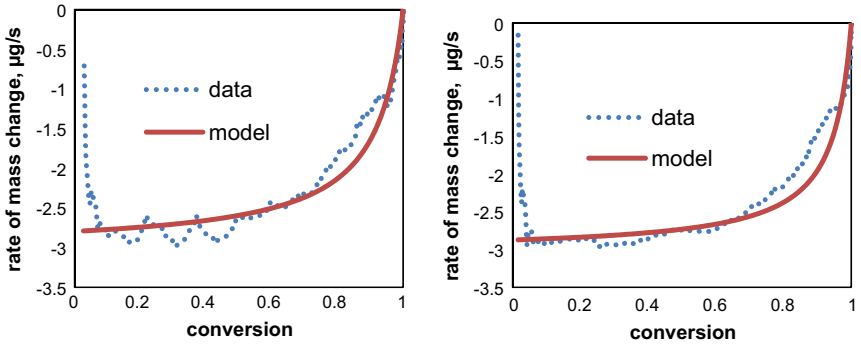

Fig. 6. Model predictions for experiments in a taller crucible, hence lowered external mass transfer coefficient. Left: particle size 300–425 µm, sample mass 6.44 mg; Right: particle size 300–425 µm, sample mass 9.84 mg, reaction temperature 900 °C.

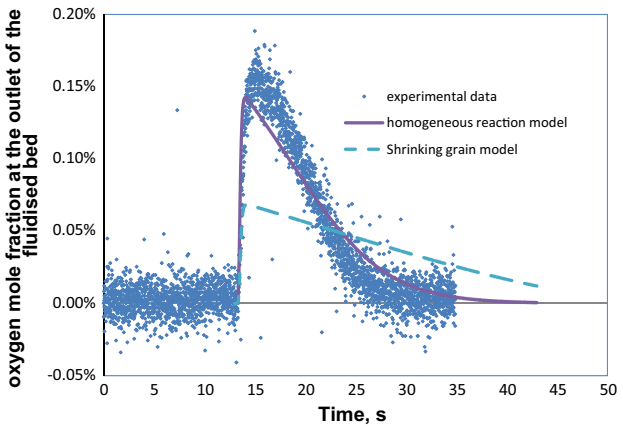

Fig. 7. Results from batch experiment in a fluidised bed: sample mass 10.0 mg; fluidising gas flowrate 2.2 l/min (at 293 K and 1 atm); bed temperature 904 °C, compared with model results using the homogeneous reaction model (solid line) and the shrinking grain model (dashed line).

$$d_b = 0.38H^{0.8}(U_0 - U_{mf})^{0.42} \times \exp[-1.4 \times 10^{-4} - 0.25(U_0 - U_{mf})^2 - 0.1(U_0 - U_{mf})] \quad (13)$$

with H being the vertical distance from the distributor.

In terms of transfer processes, the mass transfer coefficient was calculated from the Sherwood number, which was in turn estimated using the modified Frössling's equation [51], *viz.*

$$Sh = 2\varepsilon_{mf} + 0.69\left(\frac{2r_0U_{mf}}{\varepsilon_{mf}\nu}\right)^{1/2}\left(\frac{\nu}{D}\right)^{1/3}. \quad (14)$$

Here, ε_{mf} is the bed voidage at incipient fludisation, measured to be 0.42, ν is the kinematic viscosity of the fluidising gas. Within one spherical particle, the change in the concentration of oxygen, C at a distance r from the centre of the particle is governed by

$$\varepsilon_p\frac{\partial C}{\partial t} = \frac{1}{r^2}\frac{\partial}{\partial r}\left(r^2D_{eff}\frac{\partial C}{\partial r}\right) + \frac{\rho_m}{4}\frac{dX}{dt}. \quad (15)$$

The energy equation, ignoring contribution from the gas phase, is

$$c_p\frac{\partial T}{\partial t} = \frac{1}{r^2}\frac{\partial}{\partial r}\left(r^2\lambda_s\frac{\partial T}{\partial r}\right) + \frac{\rho_m}{4}\frac{dX}{dt}(-\Delta H) \quad (16)$$

where c_p is the volumetric heat capacity of the solid, T is the thermodynamic temperature at position r, λ_s is the thermal conductivity in the solid and ΔH the heat of reaction per mole of oxygen in the decomposition reaction (1).

The boundary conditions used were

$$X(0,r) = 0 \quad (17a)$$

$$C(0,r) = 0 \quad (17b)$$

$$\frac{\partial C}{\partial r}(t,0) = 0 \quad (17c)$$

$$-D_{eff}\frac{\partial C}{\partial r}\Big|_{r_0} = \frac{Sh \times D}{2r_0}(C|_{r=r_0} - C_{em}) \quad (17d)$$

$$T(0,r) = 293 \quad (17e)$$

$$\frac{\partial T}{\partial r}(t,0) = 0 \quad (17f)$$

$$-\lambda_s\frac{\partial T}{\partial r}\Big|_{r_0} = \frac{Nu \times \lambda_{N_2}}{2r_0}(T|_{r=r_0} - T_{em}) + 5.67 \times 10^{-8}(T|^4_{r=r_0} - T^4_{em}) \quad (17g)$$

where C_{em} is the concentration of oxygen in the particulate phase, T_{em} is the temperature of the particulate phase and λ_{N_2} is the thermal conductivity of nitrogen. The Nusselt number, Nu, was assumed to be 2 as a rough estimate since the uncertainties in the thermal conductivity of the solid and the black assumption of the bed overshadowed the uncertainty in Nu. However, it was found that with the estimated heat transfer parameters, the particles would heat up uniformly across its diameter, to the reaction temperature in ~0.4 s, and the temperature profile remained largely constant during the reaction. Thus the heat transfer is considered unimportant in this case. The modelling results confirmed that the reaction profile was largely uniform within the particles, consistent with the findings from Section 3.3.2. It is worth noting that Eq. (14) is applicable when the active particle is much larger than the bed material [51]. In this case, the oxygen carriers and the silica sand are comparable in size. Thus the actual Sherwood number is expected to be higher than the calculated value of 1.11. If the Sherwood number were taken to be 2 or higher, the homogeneous reaction model would be in excellent agreement with the experimental data.

Solving Eqs. (11–16) together with (4b) using different reaction models (*i.e.* different $f(X)$ and corresponding rate constants) yielded the results shown in Fig. 7. When comparing the two sets of results, it is clear that the homogeneous reaction model was able to reproduce the experimental results closely whereas the shrinking grain model underestimated the rate of reaction significantly.

5. Conclusion

Here, a 60 wt% copper-based oxygen carrier supported on inert calcium aluminate was prepared and characterised. The particles were active over repeated redox cycles at high temperatures with no apparent loss in activity. The kinetics of the decomposition of

CuO in the carrier were investigated in a TGA and a fluidised bed. It was found that:

(a) The rate of decomposition of particles in the sieve size range 300–425 μm was controlled by intrinsic chemical kinetics and external transfer of mass from the surface of the particles to the bulk gas in the TGA.
(b) The rate of reaction was unaffected by the number of times the particles had been subject to cycles of oxidation and reduction.
(c) By appropriate modelling of the various resistances, values of the rate constant for the decomposition were obtained as a function of temperature. The activation energy of the reaction was found to be 59.7 kJ/mol (with a standard error of 5.6 kJ/mol) and the corresponding pre-exponential factor was 632 m^3/mol/s.
(d) The local rate of conversion within a particle was assumed to occur either (i) by homogeneous reaction, or (ii) in uniform, non-porous grains, each reacting as a kinetically-controlled shrinking core. On the basis of experiment and theory, it was found that the homogeneous reaction model was more plausible.

A set of kinetics parameters could be determined which predicted the observed rates in both the fluidised bed and TGA experiment.

Acknowledgements

This work is supported by the Engineering and Physical Sciences Research Council (EPSRC Grant EP/I010912/1) and The Cambridge Commonwealth, European & International Trust as well as Selwyn College, University of Cambridge. The authors would also like to thank Mohammad Ismail for the XRD analysis and Zlatko Saracevic for the nitrogen adsorption analysis.

References

[1] Lyngfelt A, Leckner B, Mattisson T. A fluidized-bed combustion process with inherent CO_2 separation; application of chemical-looping combustion. Chem Eng Sci 2001;56:3101–13. http://dx.doi.org/10.1016/S0009-2509(01)00007-0.
[2] Ishida M, Jin H. CO_2 recovery in a power plant with chemical looping combustion. Energy Convers Manage 1997;38:S187–92. http://dx.doi.org/10.1016/S0196-8904(96)00267-1.
[3] Adánez J, Gayán P, Celaya J, de Diego LF, García-Labiano F, Abad A. Chemical looping combustion in a 10 kWth prototype using a CuO/Al_2O_3 oxygen carrier: effect of operating conditions on methane combustion. Ind Eng Chem Res 2006;45:6075–80. http://dx.doi.org/10.1021/ie060364l.
[4] Adánez J, de Diego LF, García-Labiano F, Gayán P, Abad A, Palacios JM. Selection of oxygen carriers for chemical-looping combustion. Energy Fuels 2004;18:371–7. http://dx.doi.org/10.1021/ef0301452.
[5] Berguerand N, Lyngfelt A. Design and operation of a 10 kWth chemical-looping combustor for solid fuels – testing with South African coal. Fuel 2008;87:2713–26. http://dx.doi.org/10.1016/j.fuel.2008.03.008.
[6] Cho P, Mattisson T, Lyngfelt A. Comparison of iron-, nickel-, copper- and manganese-based oxygen carriers for chemical-looping combustion. Fuel 2004;83:1215–25. http://dx.doi.org/10.1016/j.fuel.2003.11.013.
[7] Abad A, Adánez J, García-Labiano F, de Diego LF, Gayán P, Celaya J. Mapping of the range of operational conditions for Cu-, Fe-, and Ni-based oxygen carriers in chemical-looping combustion. Chem Eng Sci 2007;62:533–49. http://dx.doi.org/10.1016/j.ces.2006.09.019.
[8] Adánez J, Abad A, Garcia-Labiano F, Gayan P, De Diego LF. Progress in chemical-looping combustion and reforming technologies. Prog Energy Combust Sci 2012;38:215–82. http://dx.doi.org/10.1016/j.pecs.2011.09.001.
[9] Moldenhauer P, Rydén M, Mattisson T, Younes M, Lyngfelt A. The use of ilmenite as oxygen carrier with kerosene in a 300 W CLC laboratory reactor with continuous circulation. Appl Energy 2014;113:1846–54. http://dx.doi.org/10.1016/j.apenergy.2013.06.009.
[10] Rydén M, Leion H, Mattisson T, Lyngfelt A. Combined oxides as oxygen-carrier material for chemical-looping with oxygen uncoupling. Appl Energy 2014;113:1924–32. http://dx.doi.org/10.1016/j.apenergy.2013.06.016.
[11] Mattisson T, Lyngfelt A, Leion H. Chemical-looping with oxygen uncoupling for combustion of solid fuels. Int J Greenh Gas Control 2009;3:11–9. http://dx.doi.org/10.1016/j.ijggc.2008.06.002.
[12] Mattisson T, Leion H, Lyngfelt A. Chemical-looping with oxygen uncoupling using CuO/ZrO_2 with petroleum coke. Fuel 2009;88:683–90. http://dx.doi.org/10.1016/j.fuel.2008.09.016.
[13] Shulman A, Cleverstam E, Mattisson T, Lyngfelt A. Manganese/iron, manganese/nickel, and manganese/silicon oxides used in chemical-looping with oxygen uncoupling (CLOU) for combustion of methane. Energy Fuels 2009;23:5269–75. http://dx.doi.org/10.1021/ef9005466.
[14] Abad A, Adánez-Rubio I, Gayán P, García-Labiano F, de Diego LF, Adánez J. Demonstration of chemical-looping with oxygen uncoupling (CLOU) process in a 1.5 kWth continuously operating unit using a Cu-based oxygen-carrier. Int J Greenh Gas Control 2012;6:189–200. http://dx.doi.org/10.1016/j.ijggc.2011.10.016.
[15] Dennis JS, Scott SA. In situ gasification of a lignite coal and CO_2 separation using chemical looping with a Cu-based oxygen carrier. Fuel 2010;89:1623–40. http://dx.doi.org/10.1016/j.fuel.2009.08.019.
[16] Kramp M, Thon A, Hartge E-U, Heinrich S, Werther J. Carbon stripping – a critical process step in chemical looping combustion of solid fuels. Chem Eng Technol 2012;35:497–507. http://dx.doi.org/10.1002/ceat.201100438.
[17] Markström P, Linderholm C, Lyngfelt A. Chemical-looping combustion of solid fuels – design and operation of a 100 kW unit with bituminous coal. Int J Greenh Gas Control 2013;15:150–62. http://dx.doi.org/10.1016/j.ijggc.2013.01.048.
[18] Adánez-Rubio I, Abad A, Gayán P, de Diego LF, García-Labiano F, Adánez J. Identification of operational regions in the Chemical-Looping with Oxygen Uncoupling (CLOU) process with a Cu-based oxygen carrier. Fuel 2012;102:634–45. http://dx.doi.org/10.1016/j.fuel.2012.06.063.
[19] Xu L, Wang J, Li Z, Cai N. Experimental study of cement-supported CuO oxygen carriers in chemical looping with oxygen uncoupling (CLOU). Energy Fuels 2013;27:1522–30. http://dx.doi.org/10.1021/ef301969k.
[20] Wen Y, Li Z, Xu L, Cai N. Experimental study of natural Cu ore particles as oxygen carriers in chemical looping with oxygen uncoupling (CLOU). Energy Fuels 2012;26:3919–27. http://dx.doi.org/10.1021/ef300076m.
[21] Azimi G, Leion H, Mattisson T, Lyngfelt A. Chemical-looping with oxygen uncoupling using combined Mn-Fe oxides, testing in batch fluidized bed. Energy Proc 2011;4:370–7. http://dx.doi.org/10.1016/j.egypro.2011.01.064.
[22] Azimi G, Rydén M, Leion H, Mattisson T, Lyngfelt A. $(Mn_z\ Fe_{1-z})_yO_x$ combined oxides as oxygen carrier for chemical-looping with oxygen uncoupling. AIChE J 2013;59:582–8. http://dx.doi.org/10.1002/aic.13847.
[23] Gayán P, Adánez-Rubio I, Abad A, de Diego LF, García-Labiano F, Adánez J. Development of Cu-based oxygen carriers for Chemical-Looping with Oxygen Uncoupling (CLOU) process. Fuel 2012;96:226–38. http://dx.doi.org/10.1016/j.fuel.2012.01.021.
[24] Källén M, Rydén M, Dueso C, Mattisson T, Lyngfelt A. $CaMn_{0.9}Mg_{0.1}O_{3-\delta}$ as oxygen carrier in a gas-fired 10 kWth chemical-looping combustion unit. Ind Eng Chem Res 2013;52:6923–32. http://dx.doi.org/10.1021/ie303070h.
[25] Rydén M, Lyngfelt A, Mattisson T. $CaMn_{0.875}Ti_{0.125}O_3$ as oxygen carrier for chemical-looping combustion with oxygen uncoupling (CLOU)—experiments in a continuously operating fluidized-bed reactor system. Int J Greenh Gas Control 2011;5:356–66. http://dx.doi.org/10.1016/j.ijggc.2010.08.004.
[26] Arjmand M, Hedayati A, Azad A-M, Leion H, Rydén M, Mattisson T. $Ca_xLa_{1-x}Mn_{1-y}M_yO_{3-\delta}$(M = Mg, Ti, Fe, or Cu) as oxygen carriers for chemical-looping with oxygen uncoupling (CLOU). Energy Fuels 2013;27:4097–107. http://dx.doi.org/10.1021/ef3020102.
[27] Jacob KT, Alcock CB. Thermodynamics of $CuAlO_2$ and $CuAl_2O_4$ and phase equilibria in the system Cu_2O–CuO–Al_2O_3. J Am Ceram Soc 1975;58:192–5. http://dx.doi.org/10.1111/j.1151-2916.1975.tb11441.x.
[28] Chuang S, Dennis J, Hayhurst A, Scott S. Development and performance of Cu-based oxygen carriers for chemical-looping combustion. Combust Flame 2008;154:109–21. http://dx.doi.org/10.1016/j.combustflame.2007.10.005.
[29] Clayton CK, Whitty KJ. Measurement and modeling of decomposition kinetics for copper oxide-based chemical looping with oxygen uncoupling. Appl Energy 2014;116:416–23. http://dx.doi.org/10.1016/j.apenergy.2013.10.032.
[30] Imtiaz Q, Kierzkowska AM, Müller CR. Coprecipitated, copper-based, alumina-stabilized materials for carbon dioxide capture by chemical looping combustion. ChemSusChem 2012;5:1610–8. http://dx.doi.org/10.1002/cssc.201100694.
[31] Arjmand M, Keller M, Leion H, Mattisson T, Lyngfelt A. Oxygen release and oxidation rates of $MgAl_2O_4$-supported CuO oxygen carrier for chemical-looping combustion with oxygen uncoupling (CLOU). Energy Fuels 2012;26:6528–39. http://dx.doi.org/10.1021/ef3010064.
[32] Imtiaz Q, Broda M, Müller CR. Structure–property relationship of co-precipitated Cu-rich, Al_2O_3- or $MgAl_2O_4$-stabilized oxygen carriers for chemical looping with oxygen uncoupling (CLOU). Appl Energy 2014;119:557–65. http://dx.doi.org/10.1016/j.apenergy.2014.01.007.
[33] De Diego LF, García-Labiano F, Gayán P, Celaya J, Palacios JM, Adánez J. Operation of a 10kWth chemical-looping combustor during 200h with a CuO–Al_2O_3 oxygen carrier. Fuel 2007;86:1036–45. http://dx.doi.org/10.1016/j.fuel.2006.10.004.
[34] Donat F, Hu W, Scott SA, Dennis JS. Characteristics of copper-based oxygen carriers supported on calcium aluminates for chemical-looping combustion with oxygen uncoupling (CLOU). Ind Eng Chem Res 2015;54:6713–23. http://dx.doi.org/10.1021/acs.iecr.5b01172.
[35] Song Q, Liu W, Bohn CD, Harper RN, Sivaniah E, Scott SA, et al. A high performance oxygen storage material for chemical looping processes with CO_2 capture. Energy Environ Sci 2013;6:288–98. http://dx.doi.org/10.1039/C2EE22801G.

[36] Adánez-Rubio I, Gayán P, Abad A, de Diego LF, García-Labiano F, Adánez J. Evaluation of a spray-dried CuO/$MgAl_2O_4$ oxygen carrier for the chemical looping with oxygen uncoupling process. Energy Fuels 2012;26:3069–81. http://dx.doi.org/10.1021/ef3002229.
[37] Sahir AH, Sohn HY, Leion H, Lighty JS. Rate analysis of chemical-looping with oxygen uncoupling (CLOU) for solid fuels. Energy Fuels 2012;26:4395–404. http://dx.doi.org/10.1021/ef300452p.
[38] Clayton CK, Sohn HY, Whitty KJ. Oxidation kinetics of Cu_2O in oxygen carriers for chemical looping with oxygen uncoupling. Ind Eng Chem Res 2014;53:2976–86. http://dx.doi.org/10.1021/ie402495a.
[39] Zhao H, Liu L, Wang B, Xu D, Jiang L, Zheng C. Sol–gel-derived NiO/$NiAl_2O_4$ oxygen carriers for chemical-looping combustion by coal char. Energy Fuels 2008;22:898–905. http://dx.doi.org/10.1021/ef7003859.
[40] Liu L, Zachariah MR. Enhanced performance of alkali metal doped Fe_2O_3 and Fe_2O_3/Al_2O_3 composites as oxygen carrier material in chemical looping combustion. Energy Fuels 2013;27:4977–83. http://dx.doi.org/10.1021/ef400748x.
[41] Liu W, Ismail M, Dunstan MT, Hu W, Zhang Z, Fennell PS, et al. Inhibiting the interaction between FeO and Al_2O_3 during chemical looping production of hydrogen. RSC Adv 2015;5:1759–71. http://dx.doi.org/10.1039/C4RA11891J.
[42] Saucedo MA, Butel M, Scott SA, Collings N, Dennis JS. Significance of gasification during oxy-fuel combustion of a lignite char in a fluidised bed using a fast UEGO sensor. Fuel 2015;144:423–38. http://dx.doi.org/10.1016/j.fuel.2014.10.029.
[43] Regitz S, Collings N. Fast response air-to-fuel ratio measurements using a novel device based on a wide band lambda sensor. Meas Sci Technol 2008;19:075201. http://dx.doi.org/10.1088/0957-0233/19/7/075201.
[44] Ropp RC. Group 13 (B, Al, Ga, In and Tl) alkaline earth compounds. Encyclopedia of the alkaline earth compounds. Elsevier; 2013. p. 481–635. http://dx.doi.org/10.1016/B978-0-444-59550-8.00006-5.
[45] Eagleson M. Copper (II) oxide. Concise Encycl Chem 1993;267.
[46] Fuller EN, Schettler PD, Giddings JC. New method for prediction of binary gas-phase diffusion coefficients. Ind Eng Chem 1966;58:18–27. http://dx.doi.org/10.1021/ie50677a007.
[47] Sit SP, Grace JR. Effect of bubble interaction on interphase mass transfer in gas fluidized beds. Chem Eng Sci 1981;36:327–35. http://dx.doi.org/10.1016/0009-2509(81)85012-9.
[48] Wen CY, Yu YH. A generalized method for predicting the minimum fluidization velocity. AIChE J 1966;12:610–2. http://dx.doi.org/10.1002/aic.690120343.
[49] Davidson JF, Harrison D. Fluidised particles. Cambridge: Cambridge University Press; 1963.
[50] Cai P, Schiavetti M, De Michele G, Grazzini GC, Miccio M. Quantitative estimation of bubble size in PFBC. Powder Technol 1994;80:99–109. http://dx.doi.org/10.1016/0032-5910(94)02834-6.
[51] Hayhurst AN. The mass transfer coefficient for oxygen reacting with a carbon particle in a fluidized or packed bed. Combust Flame 2000;121:679–88. http://dx.doi.org/10.1016/S0010-2180(99)00178-9.